



CHORUS

This is the accepted manuscript made available via CHORUS. The article has been published as:

## Coherent Superposition of Feshbach Dimers and Efimov Trimers

Yaakov Yudkin, Roy Elbaz, P. Giannakeas, Chris H. Greene, and Lev Khaykovich

Phys. Rev. Lett. **122**, 200402 — Published 24 May 2019

DOI: [10.1103/PhysRevLett.122.200402](https://doi.org/10.1103/PhysRevLett.122.200402)

# A coherent superposition of Feshbach dimers and Efimov trimers.

Yaakov Yudkin<sup>1</sup>, Roy Elbaz<sup>1</sup>, P. Giannakeas<sup>2</sup>, Chris H. Greene<sup>3</sup>, and Lev Khaykovich<sup>1</sup>

<sup>1</sup>*Department of Physics, QUEST Center and Institute of Nanotechnology  
and Advanced Materials, Bar-Ilan University, Ramat-Gan 5290002, Israel*

<sup>2</sup>*Max Planck Institute for the Physics of Complex Systems,  
Nöthnitzer Strasse 38, 01187 Dresden, Germany and*

<sup>3</sup>*Department of Physics and Astronomy, Purdue University, West Lafayette, Indiana 47907, USA*

(Dated: May 1, 2019)

A powerful experimental technique to study Efimov physics at positive scattering lengths is demonstrated. We use the Feshbach dimers as a local reference for Efimov trimers by creating a coherent superposition of both states. Measurement of its coherent evolution provides information on the binding energy of the trimers with unprecedented precision and yields access to previously inaccessible parameters of the system such as the Efimov trimers' lifetime and the elastic processes between atoms and the constituents of the superposition state. We develop a comprehensive data analysis suitable for noisy experimental data that confirms the trustworthiness of our demonstration.

In few-body physics, the laws of quantum mechanics allow formation of loosely bound states which possess a variety of universal properties [1] and which have been intensively explored with ultracold atoms in recent years [2–4]. In the two-body domain, weakly bound dimers are now routinely used for the characterization of Feshbach resonances [5] and for the production of ultracold molecules in their ro-vibrational ground state [6]. In the three-body domain, the captivating subject of Efimov physics has been explored in a variety of atomic systems [7–17]. But, interestingly, experimental techniques used in these explorations have been essentially limited to the study of inter-atomic inelastic processes, such as three-body recombination. Such an approach is best suited for the region of negative scattering lengths ( $a < 0$ ), where trimers can be associated from the three atom continuum. In contrast, for positive scattering lengths ( $a > 0$ ) the presence of dimers shifts the recombination loss features into the atom-dimer continuum and Efimov resonances remain inaccessible for direct observation.

One of the central results of experimental research reveals an intriguing universality in the absolute position of the Efimov resonance across diverse open-channel-dominated Feshbach resonances [14, 18–20]. The Efimov resonance's position is determined by the three-body parameter (3BP) which had generally been accepted to be nonuniversal. However, following the experimental urge, it was shown that its universality stems from the fact that atoms interact through a van der Waals potential which suppresses the probability to find the particles at short distances from each other [21–26]. The break-down of this universality has been predicted [27–29] and confirmed [17] to occur only near closed-channel-dominated Feshbach resonances.

The Efimov-van der Waals universality is well established for  $a < 0$ . However, for  $a > 0$  the presence of an atom-dimer continuum obscures the situation. The way the dimers are created in experiments poses challenges to the preparation of an initial atom-dimer mixture with a significant population of dimers. Among the vari-

ous laser-cooled bosonic species only cesium allowed the preparation of a suitable atom-dimer mixture through a rather sophisticated protocol [30, 31]. In other bosonic species Efimov resonances have been studied only indirectly by means of an avalanche mechanism [9, 11, 32–35] which is currently questioned [31, 35, 36]. From the theory side, the universality of the 3BP is predicted to weaken for  $a > 0$  [37–41]. Moreover, it predicts that the first excited Efimov level avoids merging with the atom-dimer continuum due to various finite range effects [40]. Despite continuous theoretical interest, experimental progress is hindered due to inherent limitations of the currently available experimental techniques.

In a few previous experiments a limited range of the first excited Efimov energy level has been probed by RF association [33, 42, 43]. The signature of production of Efimov trimers was revealed by loss resonances which did not permit measuring their lifetime. In addition, the finite resolution of the method prevented exploration of the vicinity of the atom-dimer resonance [33]. Although in a recent experiment the lifetime of the Efimov trimer has been measured directly, the applied method prevented access to spectroscopic information and required a rather significant initial population of trimers [44].

This Letter demonstrates a new experimental approach to study the physics of Efimov trimers at  $a > 0$ . As illustrated in Fig. 1, we utilize a short and strong pulse of magnetic field modulation which is broad enough to create a coherent superposition state of Feshbach dimers and Efimov trimers. After a variable time of its coherent evolution we apply a second pulse to observe the accumulated phase difference between the two constituents of the superposition state. The resulting oscillations reveal the Efimov trimer energy level with nearly 10-fold improvement in precision and much higher resolution limit compared to the previously applied experimental method [33]. Even more importantly, we observe the decay of the coherent oscillations which can be related to different decoherence mechanisms such as the trimers' lifetime and the elastic atom-dimer and/or atom-trimer collision rates. Note, finally, that we benefit from the

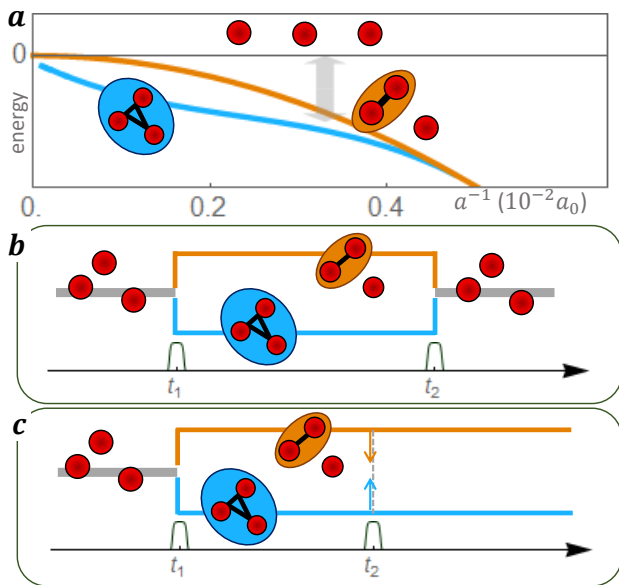


FIG. 1. **Illustration of the energy levels and of the interferometer.** **a.** The dimer (orange) and trimer (blue) energy levels (not to scale) are shown schematically as a function of the inverse scattering length. The grey arrow indicates the parameter regime of our work and illustrates the effect of the modulation pulse. **b,c.** The two pulse sequence results in constructive (b) or destructive (c) interference.

four-fold interferometric enhancement of the signal and demonstrate high sensitivity in probing a small population of trimers.

The experiment is performed on  ${}^7\text{Li}$  atoms, polarized in the  $|F=1, m_F=0\rangle$  state and evaporatively cooled to a temperature of  $T \approx 1.5 \mu\text{K}$  in a crossed-beam optical trap in the vicinity of a Feshbach resonance [45]. The magnetic field bias is set to 880.25 G which corresponds to a scattering length of  $\sim 300a_0$  and a Feshbach dimer binding energy of  $E_d = -h \times 6 \text{ MHz}$  [see Fig. 1(a)] [46]. According to an earlier study described in Ref. [33], the first excited Efimov trimer energy level is predicted to be just  $\sim 100 \text{ kHz}$  below  $E_d$ , i.e.  $E_t - E_d \approx -h \times 100 \text{ kHz}$ , where  $E_t$  is the energy of the trimer state. In Ref. [33],  $E_t - E_d$  was measured in the region of  $0.5 \text{ MHz} < E_d/h < 4 \text{ MHz}$  by means of loss spectroscopy. The frequency dependent magnetic field modulation was applied for tens to hundreds of ms, and the induced atom loss resonances were related to the positions of dimer and trimer energy levels. The accessible region of the trimer's binding energies was constrained by the finite resolution limit to be  $\gtrsim 110 \text{ kHz}$ . Thus, our current measurement probes the region which was out of reach for the previous experimental technique.

The concept of the interferometer relies on a clear separation of energy scales in the system:  $E_d \gg E_t - E_d > k_B T$ . The first step of the interferometer, shown in Fig. 1(b,c), is the beam-splitter at time  $t_1$ . The bias field is modulated at  $\nu_m = 6 \text{ MHz}$  for a FWHM duration

of  $\tau_m = 10 \mu\text{s}$  by a single auxiliary coil. The modulation amplitude at the atom position is  $b \approx 1.5 \text{ G}$  [45]. The Fourier transform limited bandwidth of the pulse is  $100 \text{ kHz}$  at FWHM which allows us to address both (dimer and trimer) energy levels simultaneously while covering the full thermal distribution of the free-atom continuum ( $\sim 30 \text{ kHz}$  for  $T \approx 1.5 \mu\text{K}$ ). The pulse projects the three-atom continuum to a coherent superposition state of a dimer + free atom and a trimer, denoted hereafter as DITRIS (DImer-TRImer Superposition) state. The system then evolves freely for a variable time  $t \gg \tau_m$  during which the two constituents of the DITRIS accumulate a relative phase difference of  $\phi(t) = (E_t - E_d)t/\hbar$ , assuming that the energy of the free atom in the dimer + atom pathway is negligible (see the discussion of the results below). At time  $t_2 = t_1 + t$  an identical modulation pulse projects the two paths back to free atoms and serves as an output port of the interferometer. When  $\phi(t) = 2\pi n$ , where  $n \in \mathbb{Z}$ , constructive interference between the two paths projects the three atoms into the three-atom continuum as shown in Fig. 1(b). In contrast, Fig. 1(c) represents the case where  $\phi(t) = \pi(2n+1)$  when destructive interference suppresses dissociation of the bound states. This produces a time dependent periodic variation in the number of free atoms with a peak-to-peak amplitude proportional to  $N_D$ , where  $N_D$  is the number of DITRIS states produced by the first pulse. This two-path interferometer picture neglects the contribution of the third path where the three atoms remain in the three-atom continuum. However, due to our experimental conditions ( $E_d \gg E_t - E_d$ ) this channel contributes oscillations at  $\sim E_d/h$  which are averaged to zero in the range of interest, namely  $(E_t - E_d)/h$  [45].

The results of our interferometer at the output port are shown in Fig. 2, where we measure the number of free atoms,  $N(t)$ , as a function of the free evolution time  $t$ . Each point represents the mean of 2 - 8 individual measurements. It is evident from the data that the signal-to-noise ratio (SNR) is small. We, hence, begin the analysis with the data for short evolution times [ $80 \mu\text{s} < t < 220 \mu\text{s}$ ; Fig. 2(a)], where the oscillations can be visually appreciated. Assuming constant amplitude oscillations, we apply three different analyses: (i) a fast Fourier transform (FFT), and (ii) a two- and (iii) a three-parameter fit to the cosine function:

$$\frac{N(t)}{N_0} = 1 + A \cos(2\pi\nu t + \varphi), \quad (1)$$

where  $N_0$  is the initial number of atoms in the trap. In (ii), the two fitting parameters are the amplitude  $A$  and the phase  $\varphi$ , while in (iii) the frequency  $\nu$  becomes the third fitting parameter.

We verify that in case of small SNR, the most stringent test for the claim that an oscillation frequency has been observed in the experiment is provided by the three-parameter fit, and, therefore, only this analysis is discussed below [45]. The fitting algorithm is applied to the experimental results using a variety of initial con-

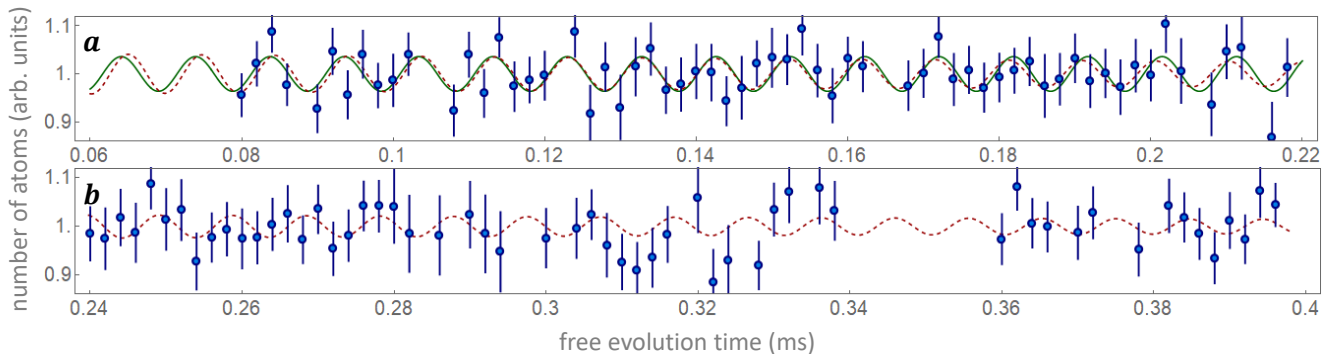


FIG. 2. **Observation of oscillations.** The number of free atoms  $N$  after the interferometer sequence is measured as a function of the free evolution time  $t$ . Each data point is the average of 2 – 8 measurements and the error bar is  $1\sigma$  of the mean error. **a.** Data for  $t \in [80, 220] \mu\text{s}$ . The green line is the best fit to a cosine. **b.** Data for  $t \in [240, 400] \mu\text{s}$ . The red dashed line in **a.** and **b.** is (one and the same) best fit to a decaying cosine.

ditions. In particular, the initial frequency is scanned very densely in the relevant frequency range. However, the fitting algorithm converges only to a limited number of frequencies, all of which are shown in Fig. 3(I). Among all the converged frequencies, only  $\nu^* = 102.9(8)$  kHz [47] has a distinguishable amplitude  $A^* = 0.036(7)$ , while all other  $A(\nu)$  are smaller and similar to each other [see Fig. 3(I)(a)]. This provides the first evidence that a single, dominant frequency can be indicated in the data. In fact, a naturally defined  $\text{SNR} = A^*/\bar{A}$ , where  $\bar{A}$  is the mean value of  $A(\nu)$  excluding  $A^*$ , is found to be  $\text{SNR} = 2.79(55)$ . The second evidence for the presence of a dominant frequency is the coincidence of global minima in errors obtained for all three fitting parameters at  $\nu^*$  [see Fig. 3(I)(c,d,e)].

The reported SNR is small mainly due to the small signal that we are detecting (see discussion below), and it poses an obvious question: What is the likelihood to observe a similar peak with the same frequency analysis for a randomly generated noisy data? This is exactly the question where the full strength of the three-parameter fit method is revealed [45]. We perform a likelihood analysis with 1000 fake sequences of  $N(t)$  with the same sampling frequency and length as in Fig. 2(a) generated from a random Gaussian distribution with the same standard deviation as in our experimental data. We then apply our frequency analysis for each sequence and look for events with a SNR larger than  $1\sigma$  below the experimental SNR and a central frequency within the expected interval of [90, 110] kHz. The likelihood analysis results in zero such events. Only when the SNR-threshold is lowered to 2.1 ( $1.25\sigma$  below the experimental SNR) the first false positive occurs. Hence the probability of our result being wrong is  $0.21 \times 0.001 = 2 \times 10^{-4}$  (0.21 is the probability of getting a result  $\geq 1.25\sigma$ ). This sufficiently negligible probability together with the fact that no oscillations were detected when only a single pulse was applied [45] allows us to fully trust our results.

To see the duration of the coherent oscillations, the

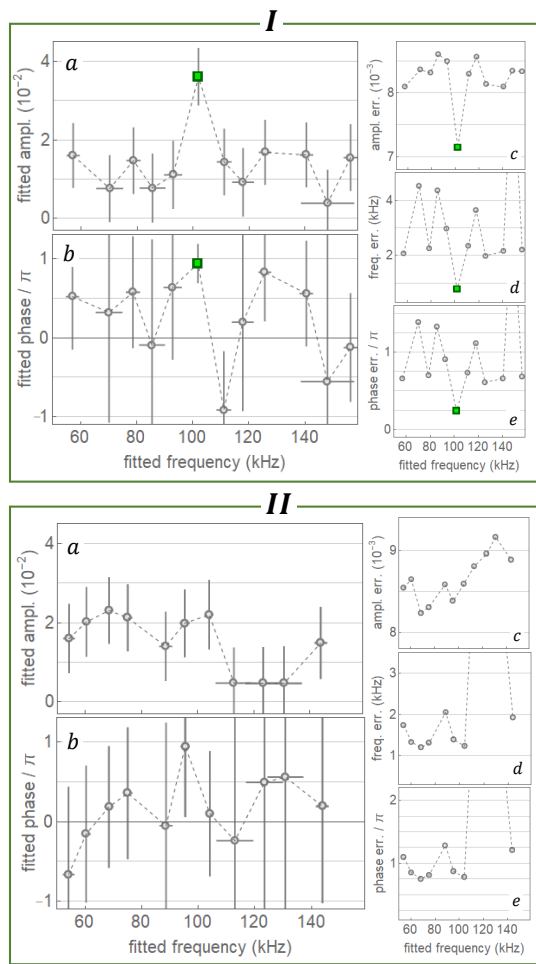


FIG. 3. **Data analysis using three free parameters. I.** The results of a three-parameter fit using the data of Fig. 2(a) and Eq. (1): **(a)**  $A(\nu)$  and **(b)**  $\varphi(\nu)$ . The error bars are  $1\sigma$  fitting uncertainties and they are also depicted in **(c)**, **(d)** and **(e)** as a function of  $\nu$ . The parameters indicated by the green square are used for the green fit in Fig. 2(a). **II.** Same as **(I)** for the data of Fig. 2(b).

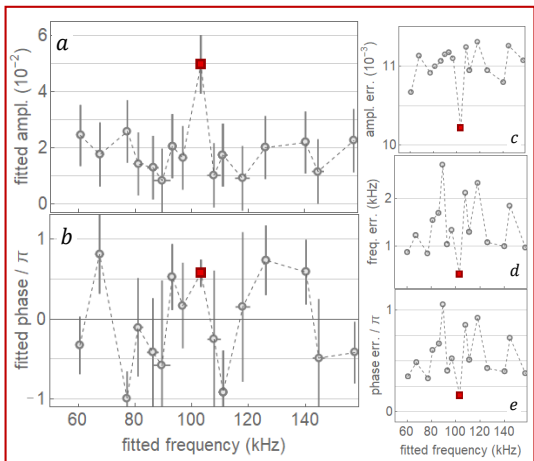


FIG. 4. **Data analysis using three free parameters and a decaying cosine.** Same as Fig. 3, but for the entire data set [Fig. 2(a+b)] and using Eq. (2) for the fit. The parameters indicated by the red square are used for the red (dashed) fit in Fig. 2.

experiment is repeated for longer free evolution times. In Fig. 2(b) the data points for  $t$  between 240  $\mu\text{s}$  and 400  $\mu\text{s}$  are shown, and the corresponding three-parameter fit analysis is in Fig. 3(II). Since we observe no dominant contribution at any frequency we conclude that the oscillations are below the detection limit and, thus, we detect the decay of the signal. Next, the entire data set ( $t \in [80, 400]$ ) is analyzed by fitting it to a damped cosine curve:

$$\frac{N(t)}{N_0} = 1 + Ae^{-t/\tau} \cos\left(t\sqrt{(2\pi\nu)^2 + \tau^{-2}} + \varphi\right). \quad (2)$$

This analysis is performed in two steps. First, a fit with four free parameters ( $A$ ,  $\tau$ ,  $\nu$  and  $\varphi$ ) is executed in the vicinity of the earlier derived values of some of them ( $A^*$ ,  $\nu^*$  and  $\varphi^*$ ). The fit converges and yields  $\tau = 331(297)$   $\mu\text{s}$  which allows us to put an upper bound of  $\sim 630$   $\mu\text{s}$  for the detected decay time. The three-parameter fit analysis is then repeated for the entire data set using Eq. (2) and keeping  $\tau = 331$   $\mu\text{s}$  fixed. The result, shown in Fig. 4, agrees with the previous one [Fig. 3(I)] for the central frequency  $\nu^*$  (within the errors) and has a slightly reduced SNR = 2.41(49). The phase of the oscillations at  $\nu^*$  is measured to be  $\varphi^* = 0.57(16)\pi$ , which is consistent with  $N(t=0) = N_0$ .

Extrapolating the damped oscillations to  $t = 0$  we obtain an initial peak-to-peak signal of  $2A = 0.10(1) \times N_0 \approx 3,000$  atoms, where  $N_0 \approx 3 \times 10^4$  is the initial number of atoms before the first pulse is applied. This implies that  $\sim 3,000/4 = 750$  atoms participate in the creation of  $\sim 750/3 = 250$  DITRIS states [45]. For our experimental parameters, a trimer-excluding theory predicts the conversion of  $\sim 0.018 \times N_0 \approx 540$  atoms into  $\sim 270$  dimers after the first pulse [48]. This provides an upper bound for

DITRIS states that can be created in our system in agreement with the observed results. Thus, the theory confirms the small signal in Fig. 2 and we fully benefit from the interferometric enhancement to obtain this level of sensitivity.

We now discuss the decay of the coherent oscillations, which can be caused by different mechanisms. The first is related to the finite thermal energy of the "spectator" atom in dimer + atom path of the interferometer. However, this scenario, if it were relevant, would cause a significantly faster decay as the thermal energy has a  $\sim 30$  kHz bandwidth. Therefore, experimental results signify a certain narrowing mechanism which currently remains unclear. This question deserves special attention, which we plan to provide in a future combined experimental and theoretical effort. On the other hand, this result opens up the opportunity to study other sources of decoherence.

The other two mechanisms indicate access to new observables, that were inaccessible in previous experiments. In the first, molecules are lost due to the finite lifetime of the trimers ( $T_1$  time). As trimers naturally have a shorter lifetime than the dimers, the contribution of the finite lifetime of the dimers can be safely excluded from consideration. In the second mechanism ( $T_2$  time) coherence is lost due to elastic collisions between the constituents of the DITRIS states and the free atoms. Our reported result sets an upper bound on both times. Future experiments should be able to determine which of the above is the dominant mechanism by analyzing the density dependence of the decoherence time  $\tau$ . The  $T_1$  time is density independent while the  $T_2$  time decreases for higher densities.

The observed decoherence is probably caused by the finite lifetime of the trimers (which seems to be longer than the previously observed lifetime in a gas of  $^{85}\text{Rb}$  atoms [44]). However, closer to the Efimov resonance the atom-dimer elastic collisional cross-section increases by several orders of magnitude and might become the dominant mechanism for decoherence. Future experiments should allow investigation of this aspect of Efimov physics which is currently totally absent from the list of available experimental observables.

In conclusion, we demonstrate the creation of a superposition state of Efimov trimers and Feshbach dimers. The newly developed data analysis, consistency in the fitting parameters and vanishingly small level of failure in the likelihood analysis prove that the interference signal between the constituents of the superposition state observed in the experiment is real. We thus measure the energy of the trimer bound state with high precision and give an upper bound for decoherence processes. The main difficulty, namely the small SNR, needs to be improved for future applications. First, by increasing the stability of the sample preparation and the detection we expect to reduce the noise by a factor of  $\sim 2$ . Second, by using a denser sample improving the signal by a factor of  $\sim 2$  is feasible.

An interesting question for future research is the identification of the exact mechanism responsible for the decoherence. Another extension of our work consists of repeating the interferometer sequence at different values of the bias field (different scattering lengths) to explore the elastic collisions channel and to identify the position of the Efimov resonance, and whether it even exists. Applying the interferometer to other accessible sub-levels of lithium atoms and other atomic species should clarify

and deepen our understanding of finite range corrections to the Efimov physics at positive scattering lengths.

**Acknowledgements** Y.Y. and L.K. acknowledge fruitful discussions with N. Navon. This research was supported in part by the Israel Science Foundation (Grant No. 1340/16), the United States-Israel Binational Science Foundation (BSF, Grant No. 2012504) and by NSF Grant No. PHY-1607180. The numerical calculations have been performed using NSF XSEDE Resource Allocation No. TG-PHY150003.

- 
- [1] E. Braaten and H.-W. Hammer, *Phys. Rep.* **428**, 259 (2006).
- [2] C. H. Greene, P. Giannakeas, and J. Pérez-Ríos, *Rev. Mod. Phys.* **89**, 035006 (2017).
- [3] P. Naidon and S. Endo, *Rep. Prog. Phys.* **80**, 056001 (2017).
- [4] J. P. D’Incao, *J. Phys. B: At. Mol. Opt. Phys.* **51**, 043001 (2018).
- [5] C. Chin, R. Grimm, P. Julienne, and E. Tiesinga, *Rev. Mod. Phys.* **82**, 1225 (2010).
- [6] J. L. Bohn, A. M. Rey, and J. Ye, *Science* **357**, 1002 (2017).
- [7] T. Kraemer, M. Mark, P. Waldburger, J. G. Danzl, C. Chin, B. Engeser, A. D. Lange, K. Pilch, A. Jaakkola, H.-C. Nägerl, and R. Grimm, *Nature* **440**, 315 (2006).
- [8] A. N. Wenz, T. L. T. Ottenstein, G. Z. F. Serwane, and S. Jochim, *Phys. Rev. A* **80**, 040702(R) (2009).
- [9] M. Zaccanti, B. Deissler, C. D’Errico, M. Fattori, M. Jona-Lasinio, S. Müller, G. Roati, M. Inguscio, and G. Modugno, *Nat. Phys.* **5**, 586 (2009).
- [10] N. Gross, Z. Shotan, S. Kokkelmans, and L. Khaykovich, *Phys. Rev. Lett.* **103**, 163202 (2009).
- [11] S. E. Pollack, D. Dries, and R. G. Hulet, *Science* **326**, 1683 (2009).
- [12] F. Ferlaino, S. Knoop, M. Berninger, W. Harm, J. P. D’Incao, H.-C. Nägerl, and R. Grimm, *Phys. Rev. Lett.* **102**, 140401 (2009).
- [13] A. Zenesini, B. Huang, M. Berninger, S. Besler, H.-C. Nägerl, F. Ferlaino, R. Grimm, C. H. Greene, and J. von Stecher, *New J. Phys.* **15**, 043040 (2013).
- [14] R. J. Wild, P. Makotyn, J. M. Pino, E. A. Cornell, and D. S. Jin, *Phys. Rev. Lett.* **108**, 145305 (2012).
- [15] S.-K. Tung, K. Jiménez-García, J. Johansen, C. Parker, and C. Chin, *Phys. Rev. Lett.* **113**, 240402 (2014).
- [16] R. Pires, J. Ulmanis, S. Häfner, M. Repp, A. Arias, E. D. Kuhnle, and M. Weidemüller, *Phys. Rev. Lett.* **112**, 250404 (2014).
- [17] J. Johansen, B. J. DeSalvo, K. Patel, and C. Chin, *Nat. Phys.* **13**, 731 (2017).
- [18] M. Berninger, A. Zenesini, B. Huang, W. Harm, H.-C. Nägerl, F. Ferlaino, R. Grimm, P. S. Julienne, and J. M. Hutson, *Phys. Rev. Lett.* **107**, 120401 (2011).
- [19] N. Gross, Z. Shotan, S. Kokkelmans, and L. Khaykovich, *Phys. Rev. Lett.* **105**, 103203 (2010).
- [20] S. Roy, M. Landini, A. Trenkwalder, G. Semeghini, G. Spagnolli, A. Simoni, M. Fattori, M. Inguscio, and G. Modugno, *Phys. Rev. Lett.* **111**, 053202 (2013).
- [21] J. Wang, J. P. D’Incao, B. D. Esry, and C. H. Greene, *Phys. Rev. Lett.* **108**, 263001 (2012).
- [22] Y. Wang, J. Wang, J. P. D’Incao, and C. H. Greene, *Phys. Rev. Lett.* **109**, 243201 (2012).
- [23] R. Schmidt, S. P. Rath, and W. Zwerger, *Eur. Phys. J B* **85**, 386 (2012).
- [24] P. Naidon, S. Endo, and M. Ueda, *Phys. Rev. Lett.* **112**, 105301 (2014).
- [25] D. Blume, *Few-Body Syst.* **56**, 859 (2015).
- [26] C. Langmack, R. Schmidt, and W. Zwerger, *Phys. Rev. A* **97**, 033623 (2018).
- [27] D. S. Petrov, *Phys. Rev. Lett.* **93**, 143201 (2004).
- [28] A. O. Gogolin, C. Mora, and R. Egger, *Phys. Rev. Lett.* **100**, 140404 (2008).
- [29] P. K. Sorensen, D. V. Fedorov, A. S. Jensen, and N. T. Zinner, *Phys. Rev. A* **86**, 052516 (2012).
- [30] S. Knoop, F. Ferlaino, M. Berninger, M. Mark, H.-C. Nägerl, and R. Grimm, *Nat. Phys.* **5**, 227 (2009).
- [31] A. Zenesini, B. Huang, M. Berninger, H.-C. Nägerl, F. Ferlaino, and R. Grimm, *Phys. Rev. A* **90**, 022704 (2014).
- [32] P. Dyke, S. E. Pollack, and R. G. Hulet, *Phys. Rev. A* **88**, 023625 (2013).
- [33] O. Machtey, Z. Shotan, N. Gross, and L. Khaykovich, *Phys. Rev. Lett.* **108**, 210406 (2012).
- [34] O. Machtey, D. A. Kessler, and L. Khaykovich, *Phys. Rev. Lett.* **108**, 130403 (2012).
- [35] M.-G. Hu, R. S. Bloom, D. S. Jin, and J. M. Goldwin, *Phys. Rev. A* **90**, 013619 (2014).
- [36] C. Langmack, D. H. Smith, and E. Braaten, *Phys. Rev. A* **86**, 022718 (2012).
- [37] A. Kievsky and M. Gattobigio, *Phys. Rev. A* **87**, 052719 (2013).
- [38] C. Ji, E. Braaten, D. R. Phillips, and L. Platter, *Phys. Rev. A* **92**, 030702 (2015).
- [39] P. Giannakeas and C. H. Greene, *Few-Body Syst.* **58**, 20 (2017).
- [40] P. M. Mestrom, J. Wang, C. H. Greene, and J. P. D’Incao, *Phys. Rev. A* **95**, 032707 (2017).
- [41] P. M. A. Mestrom, T. Secker, R. M. Kroeze, and S. J. J. M. F. Kokkelmans, *Phys. Rev. A* **99**, 012702 (2019).
- [42] T. Lompe, T. B. Ottenstein, F. Serwane, A. Wenz, G. Zürn, and S. Jochim, *Science* **330**, 940 (2010).
- [43] S. Nakajima, M. Horikoshi, T. Mukaiyama, P. Naidon, and M. Ueda, *Phys. Rev. Lett.* **106**, 143201 (2011).
- [44] C. E. Klauss, X. Xie, C. Lopez-Abadia, J. P. D’Incao, Z. Hadzibabic, D. S. Jin, and E. A. Cornell, *Phys. Rev. Lett.* **119**, 143401 (2017).

- [45] See Supplementary Material at [URL will be inserted by publisher] for the experiment details, the interferometer principles and the thorough discussion of the three methods applied for the data analysis, including the likelihood analysis.
- [46] N. Gross, Z. Shotan, O. Machtey, S. Kokkelmans, and L. Khaykovich, C.R. Physique **12**, 4 (2011).
- [47] All errors reported in brackets are the  $1\sigma$  fitting errors.
- [48] P. Giannakeas, L. Khaykovich, J.-M. Rost, and C. H. Greene, **arXiv:1903.01389**.